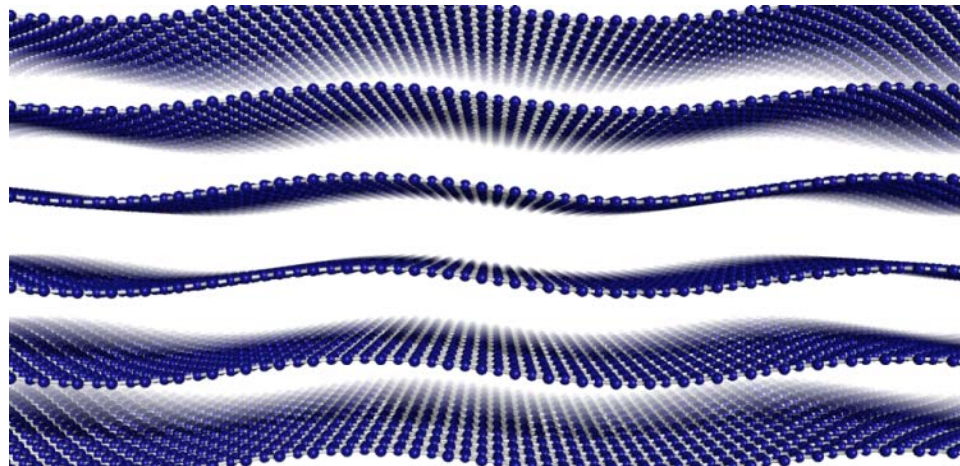


Bending Modes, Elastic Constants and Mechanical Stability of Graphitic Systems

Gianluca Savini

University of Sussex and Radboud University Nijmegen



Outline

- 1) Introduction
- 2) Elastic constants and Bending Modes
- 3) Elastic constants in graphitic systems
- 4) Conclusions

Why study layered graphitic systems

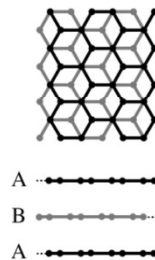
- Graphitic systems are used for many industrial applications ranging from refractory materials to neutron moderator in nuclear fission reactor and plasma shield for the next generation of fusion reactor;
- The discovery of the unusual electronic properties of graphene has raised the interest on bulk graphitic system as a route to produce graphene samples of high quality and in large scale;
- Experiments have suggested that stacking misorientations may decouple the layers giving rise to a quasi 2D electronic systems in turbostratic graphite (massless Dirac quasiparticles & quantum Hall effect)

Samples:

Kish graphite



AB-stacking graphite (**hex-g**)



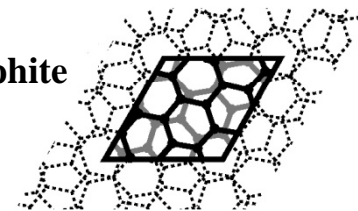
Samples:

Highly Oriented Pyrolytic Graphite

(HOPG)



Turbostratic graphite (**turbo-g**)



Why study the elastic constants

- a) Their values are decisive in engineering design to avoid material failure;
- b) They affect the mechanism of exfoliation that are relevant for the production of graphene;
- c) They strongly affect the thermodynamic properties due to a low-lying branch of acoustic vibrations, the bending modes, predicted by Lifshitz over fifty years ago [1];
- d) The knowledge of the elastic constant values is unexpected poor ;

[1] I. M. Lifshitz, Zh. Eksp. Teor. Fiz. 22, 475 (1952)

Experimental Studies

	hex-g (AB)	turbo-g
	Exp. (Bosak <i>et al.</i>)	Exp. (Blakslee <i>et al.</i>)
C_{11}	1109 ± 16	1060 ± 20
C_{12}	139 ± 36	180 ± 20
C_{33}	38.7 ± 7	36.5 ± 1
C_{13}	0 ± 3	15 ± 5
C_{44}	5.0 ± 3.0	$0.18 / 0.35$

Table I: Experimental elastic constant values for hexagonal (AB stacking) and turbostratic graphitic systems (unit of GPa).

A. Bosak *et al.*, Phys. Rev. B **75**, 153408 (2007)

O.L. Blakslee *et al.*, J. Appl. Phys. **41**, 3373 (1970)

- By imposing that the elastic strain energy as positively definite, the stability conditions are given by:

$$2C_{13}^2 < C_{33} (C_{11} + C_{12}) \quad C_{11}, C_{12}, C_{33}, C_{44} > 0$$

Elastic constants \Leftrightarrow Bending Modes

Dispersion law for the out-of-plane acoustic mode:

$$\rho \times \omega^2 (q) = C_{44} (q_x^2 + q_y^2) + C_{33} q_z^2 + \kappa (q_x^2 + q_y^2)^2 / c$$

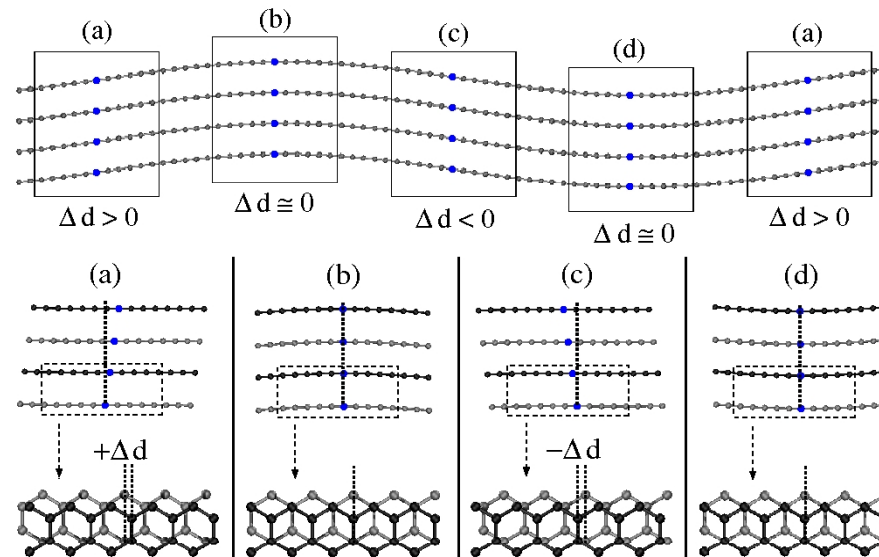


Figure 1: Transversal acoustic (bending) mode. The bending changes the local stacking between graphitic layers. The boxes (a-d) show regions with different slopes and stackings.

Elastic constants \Leftrightarrow Bending Modes

Dispersion law for the out-of-plane acoustic mode:

$$\rho \times \omega^2 (q) = C_{44} (q_x^2 + q_y^2) + C_{33} q_z^2 + \kappa (q_x^2 + q_y^2)^2 / c$$

Using trigonometric considerations, the maximum shear stacking value is:

$$\Delta d = \frac{\pi \hat{a} c}{\lambda} \times \frac{1}{\sqrt{1 + \left(\frac{2\pi \cdot \hat{a}}{\lambda} \right)^2}}$$

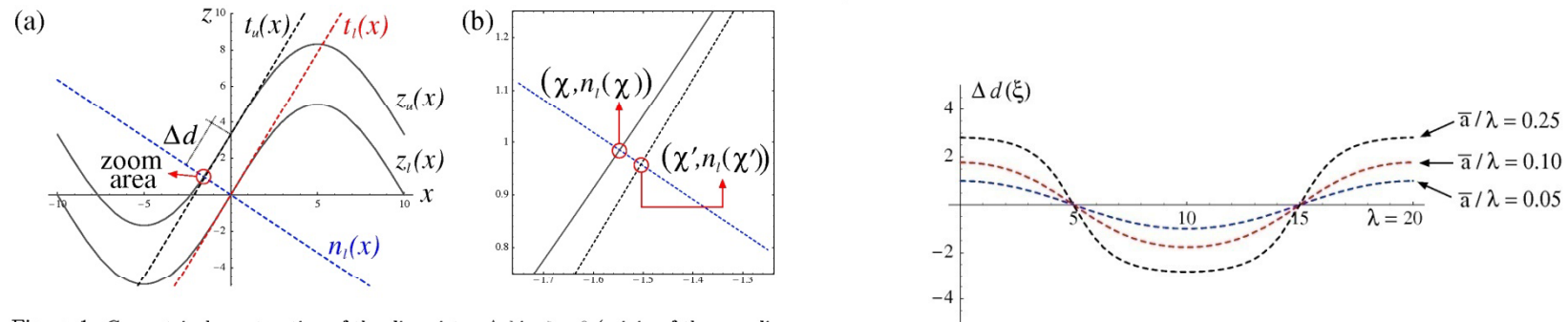


Figure 1: Geometrical construction of the disregistry Δd in $\xi = 0$ (origin of the coordinate system). (a) The black $t_u(x)$ and red $t_l(x)$ dashed line are the tangent lines in $\xi = 0$ for the upper $z_u(x)$ and lower $z_l(x)$ plane respectively (black lines). The blue dashed line $n_l(x)$ is the normal line of the lower plane in $\xi = 0$. (b) Zoom of the cross area (red circle in caption a). The cross point $(\chi, n_l(\chi))$ is the intersection between the normal line $n_l(x)$ and the upper plane $z_u(x)$. The approximate cross point $(\chi', n_l(\chi'))$ is the intersection between the lower normal line $n_l(x)$ and the upper tangent line $t_u(x)$.

Figure 1: Disregistry function $\Delta d(\xi)$ for different \bar{a}/λ ratio. For $\bar{a}/\lambda \sim 0$ the disregistry function is approaching a cosine function with amplitude $(\pi \cdot \bar{a} \cdot c)/\lambda$

Theoretical Framework

- Density-functional theory within Local Density Approximation (LDA)
 - 1) ABINIT package:
Plane waves with cut-off energy of 150 Ry
 - 2) AIMPRO package:
Localized basis-set composed of s , p and d Gaussian orbitals
 - 3) FIREBALL package:
Localized basis-set and second-order perturbation theory to include van der Waals interactions within LDA

The k -point mesh was chosen so that the average density for all computed structures correspond to 32x32x16 mesh for hex-g.

Methods to determine the elastic constants

- **Response-function:**

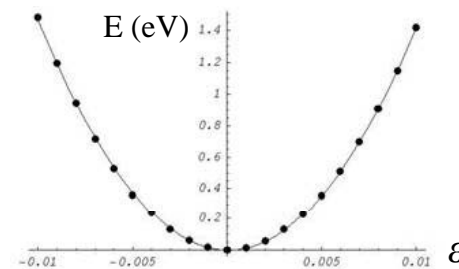
To calculate the 2nd derivate of the total energy with respect to the strain components, and then the elastic constants C_{ij}

- **Elastic density energy:**

$$w = \frac{1}{2} \sum_{i=1}^6 \sum_{j=1}^6 C_{ij} \varepsilon_i \varepsilon_j$$

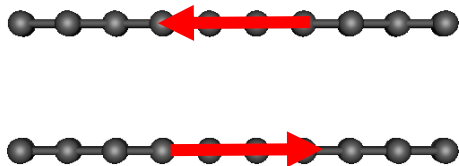
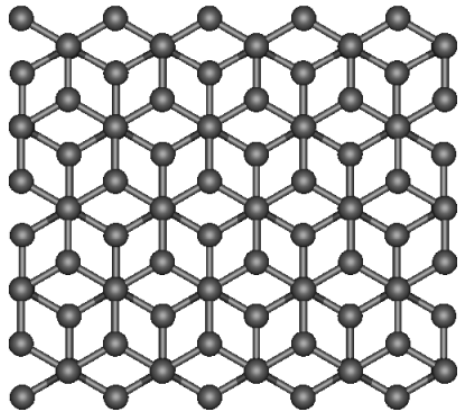
For each elastic constant we have applied 21 strain components ε_{ij} to the equilibrium structures and the atomic positions were allowed to relax.

The C_{ij} were determined by fitting the calculated total energy to a 6-order polynomial function in the strains:

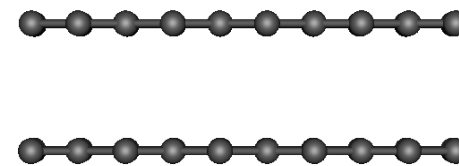
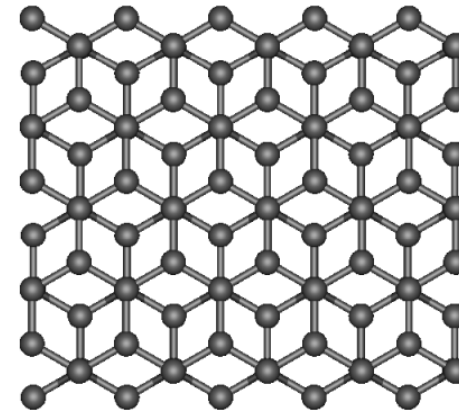


Elastic constant C_{44} , C_{13}

C_{44} = describes shear
between graphitic layers

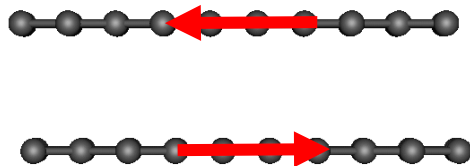
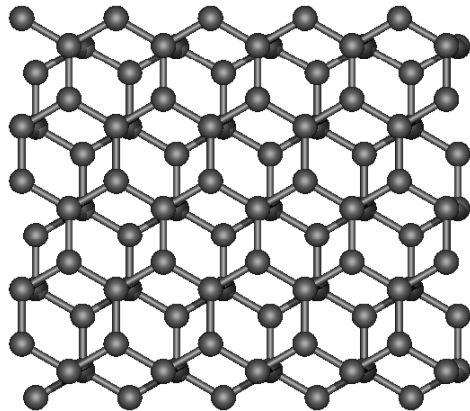


C_{13} = deformations along
basal plane and c -axis

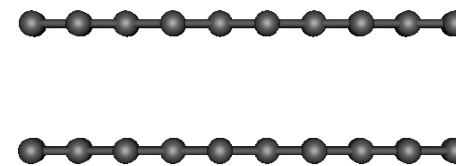
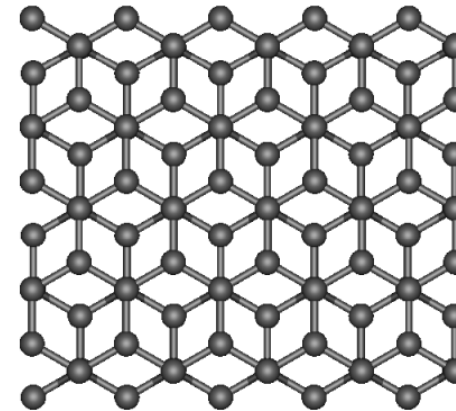


Elastic constant C_{44} , C_{13}

C_{44} = describes shear
between graphitic layers

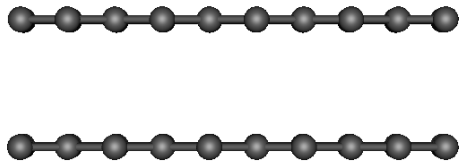
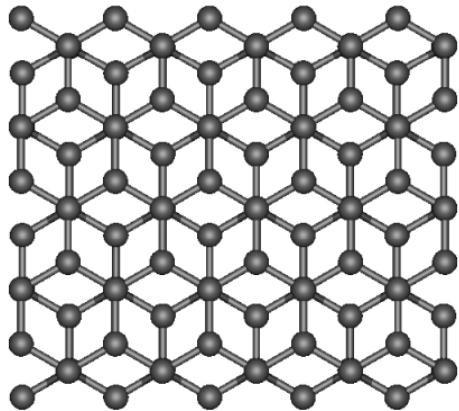


C_{13} = deformations along
basal plane and c -axis

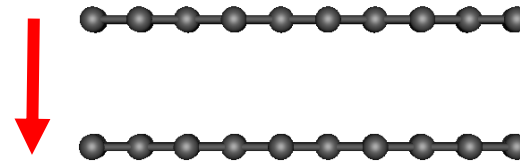
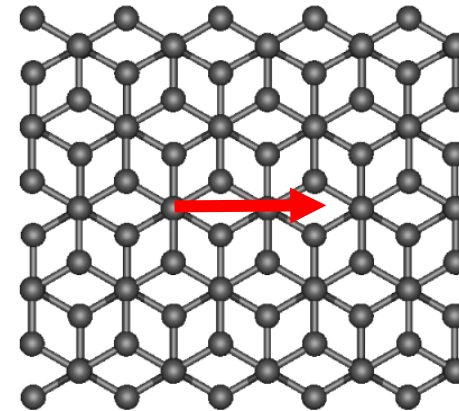


Elastic constant C_{44} , C_{13}

C_{44} = describes shear
between graphitic layers

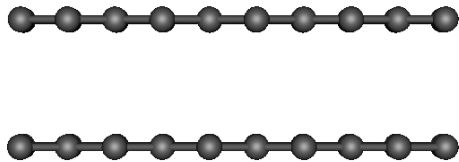
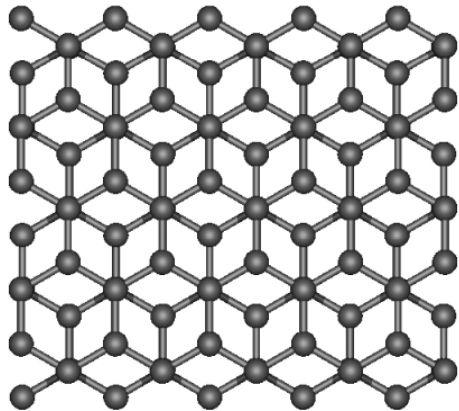


C_{13} = deformations along
basal plane and c -axis

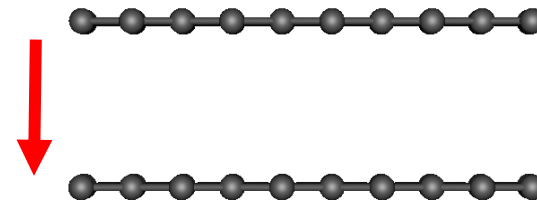
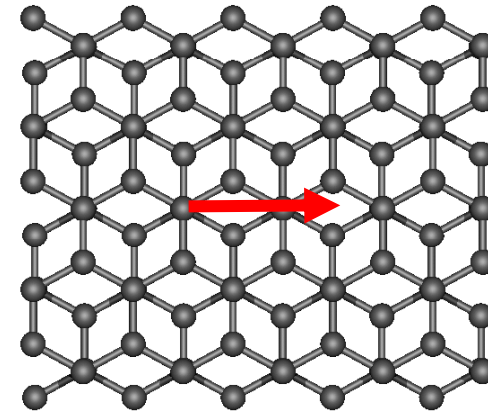


Elastic constant C_{44} , C_{13}

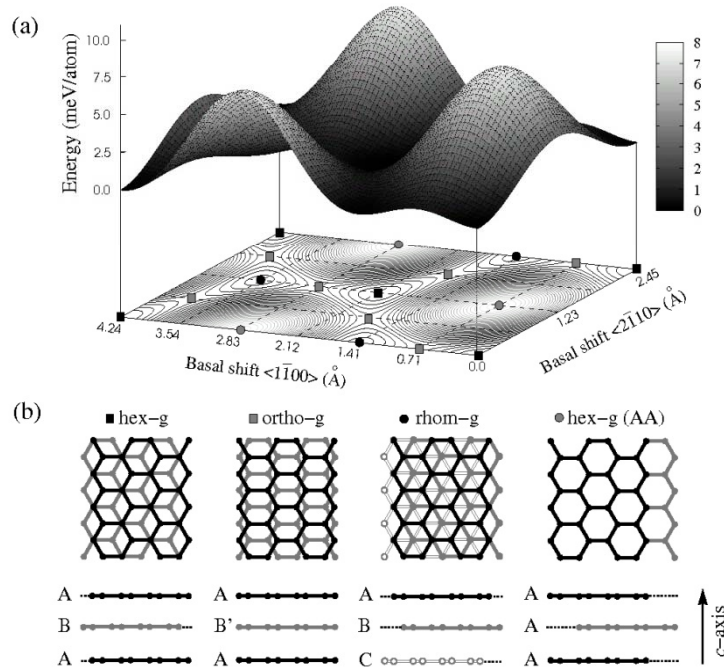
C_{44} = describes shear
between graphitic layers



C_{13} = deformations along
basal plane and c -axis



Results



	a_0 [Å]	\bar{c}_0 [Å]	E_f [meV/atom]
hex-g (AB)	2.450	3.34	0.00 (0.00)
rhombo-g	2.450	3.34	0.10 (0.10)
turbo-g	2.450	3.42	3.03 (4.63)
ortho-g	2.450	3.37	1.66 (2.05)
hex-g (AA)	2.450	3.60	9.29 (7.70)

Table I: Intralayer a_0 and interlayer \bar{c}_0 repeat distances for the five graphitic systems. The last column shows the relative formation energies E_f per atom. The value between brackets are calculated using the van der Waals corrections.

Figure 1: (a) Stacking-fault energy surface. The square and circle symbols indicate the stationary points corresponding to the following high-symmetric structures; (b) The hexagonal, orthorhombic, rhombohedral and AA hexagonal graphite viewed perpendicular (above), parallel (below) to the c -axis.

Results

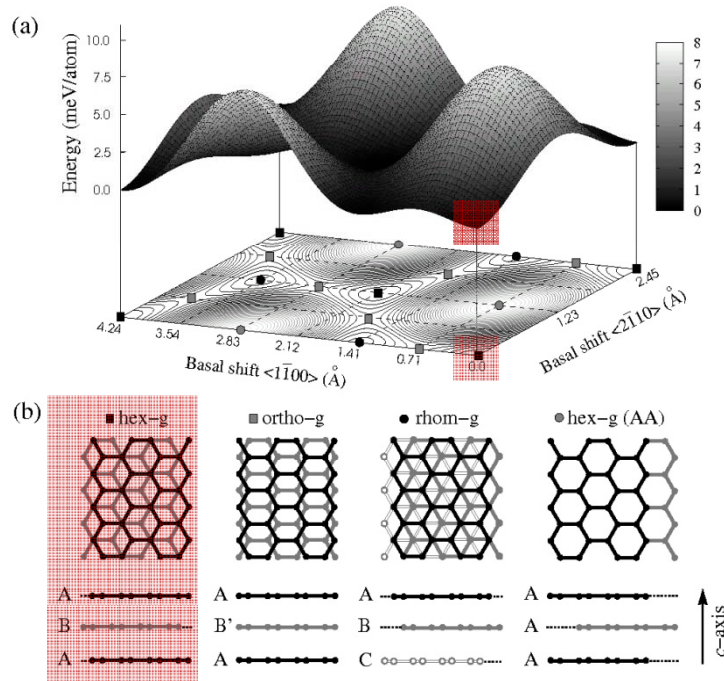


Figure 1: (a) Stacking-fault energy surface. The square and circle symbols indicate the stationary points corresponding to the following high-symmetric structures; (b) The hexagonal, orthorhombic, rhombohedral and AA hexagonal graphite viewed perpendicular (above), parallel (below) to the c -axis.

	a_0 [Å]	\bar{c}_0 [Å]	E_f [meV/atom]
hex-g (AB)	2.450	3.34	0.00 (0.00)
rhomb-g	2.450	3.34	0.10 (0.10)
turbo-g	2.450	3.42	3.03 (4.63)
ortho-g	2.450	3.37	1.66 (2.05)
hex-g (AA)	2.450	3.60	9.29 (7.70)

Table I: Intralayer a_0 and interlayer \bar{c}_0 repeat distances for the five graphitic systems. The last column shows the relative formation energies E_f per atom. The value between brackets are calculated using the van der Waals corrections.

Our work:

$$C_{44} = 4.5 \text{ GPa (Exp. } 5.0 \pm 3 \text{ GPa)}$$

$$C_{13} = -2.5 \text{ GPa (Exp. } 0 \pm 3 \text{ GPa)}$$

Results

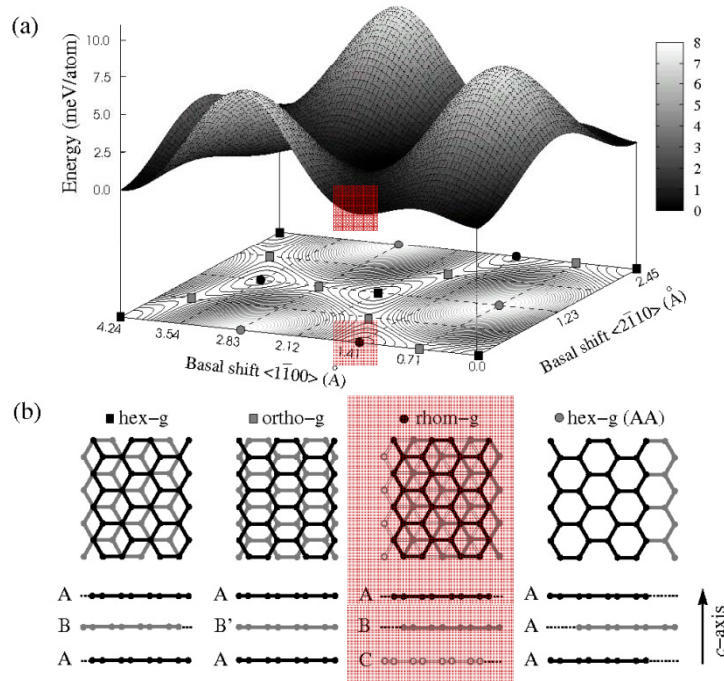


Figure 1: (a) Stacking-fault energy surface. The square and circle symbols indicate the stationary points corresponding to the following high-symmetric structures; (b) The hexagonal, orthorhombic, rhombohedral and AA hexagonal graphite viewed perpendicular (above), parallel (below) to the c -axis.

	a_0 [Å]	\bar{c}_0 [Å]	E_f [meV/atom]
hex-g (AB)	2.450	3.34	0.00 (0.00)
rhomb-g	2.450	3.34	0.10 (0.10)
turbo-g	2.450	3.42	3.03 (4.63)
ortho-g	2.450	3.37	1.66 (2.05)
hex-g (AA)	2.450	3.60	9.29 (7.70)

Table I: Intralayer a_0 and interlayer \bar{c}_0 repeat distances for the five graphitic systems. The last column shows the relative formation energies E_f per atom. The value between brackets are calculated using the van der Waals corrections.

Our work:

$$C_{44} = 4.4 \text{ GPa}$$

$$C_{13} = -2.5 \text{ GPa}$$

Results

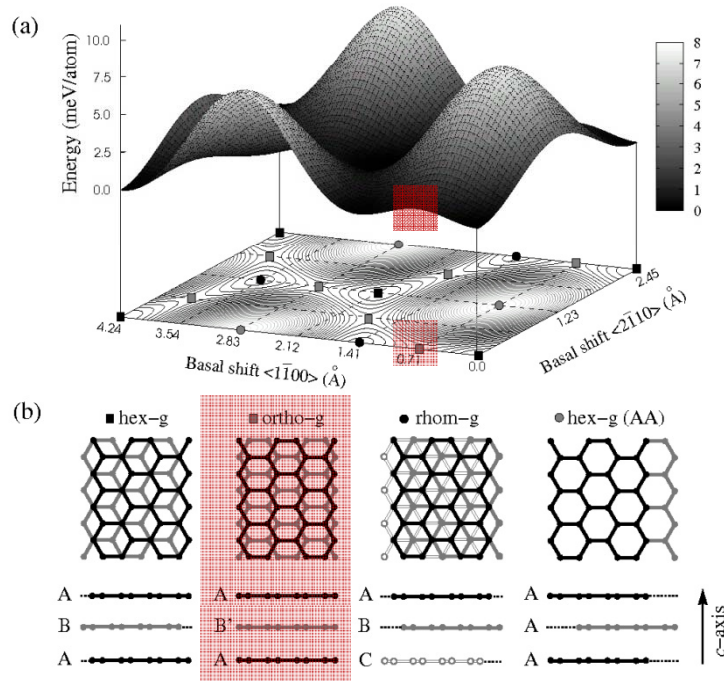


Figure 1: (a) Stacking-fault energy surface. The square and circle symbols indicate the stationary points corresponding to the following high-symmetric structures; (b) The hexagonal, orthorhombic, rhombohedral and AA hexagonal graphite viewed perpendicular (above), parallel (below) to the c -axis.

	a_0 [Å]	\bar{c}_0 [Å]	E_f [meV/atom]
hex-g (AB)	2.450	3.34	0.00 (0.00)
rhombo-g	2.450	3.34	0.10 (0.10)
turbo-g	2.450	3.42	3.03 (4.63)
ortho-g	2.450	3.37	1.66 (2.05)
hex-g (AA)	2.450	3.60	9.29 (7.70)

Table I: Intralayer a_0 and interlayer \bar{c}_0 repeat distances for the five graphitic systems. The last column shows the relative formation energies E_f per atom. The value between brackets are calculated using the van der Waals corrections.

Our work:

Results

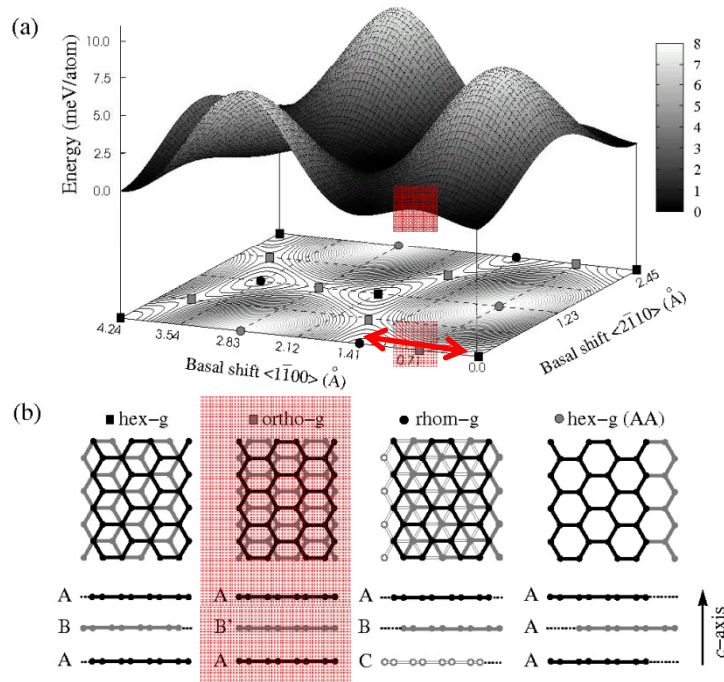


Figure 1: (a) Stacking-fault energy surface. The square and circle symbols indicate the stationary points corresponding to the following high-symmetric structures; (b) The hexagonal, orthorhombic, rhombohedral and AA hexagonal graphite viewed perpendicular (above), parallel (below) to the c -axis.

	a_0 [Å]	\bar{c}_0 [Å]	E_f [meV/atom]
hex-g (AB)	2.450	3.34	0.00 (0.00)
rhombo-g	2.450	3.34	0.10 (0.10)
turbo-g	2.450	3.42	3.03 (4.63)
ortho-g	2.450	3.37	1.66 (2.05)
hex-g (AA)	2.450	3.60	9.29 (7.70)

Table I: Intralayer a_0 and interlayer \bar{c}_0 repeat distances for the five graphitic systems. The last column shows the relative formation energies E_f per atom. The value between brackets are calculated using the van der Waals corrections.

Our work:

$$C_{44} = -2.7 \text{ GPa}$$

Results

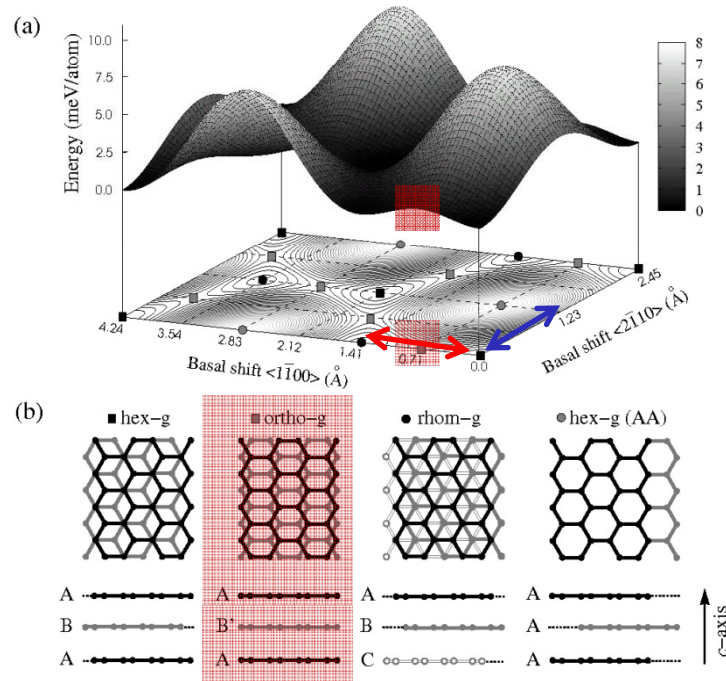


Figure 1: (a) Stacking-fault energy surface. The square and circle symbols indicate the stationary points corresponding to the following high-symmetric structures; (b) The hexagonal, orthorhombic, rhombohedral and AA hexagonal graphite viewed perpendicular (above), parallel (below) to the c -axis.

	a_0 [Å]	\bar{c}_0 [Å]	E_f [meV/atom]
hex-g (AB)	2.450	3.34	0.00 (0.00)
rhombo-g	2.450	3.34	0.10 (0.10)
turbo-g	2.450	3.42	3.03 (4.63)
ortho-g	2.450	3.37	1.66 (2.05)
hex-g (AA)	2.450	3.60	9.29 (7.70)

Table I: Intralayer a_0 and interlayer \bar{c}_0 repeat distances for the five graphitic systems. The last column shows the relative formation energies E_f per atom. The value between brackets are calculated using the van der Waals corrections.

Our work:

$$C_{44} = -2.7 \text{ GPa} \quad \text{— red line —}$$

$$C_{44} = 7.7 \text{ GPa} \quad \text{— blue line —}$$

Results

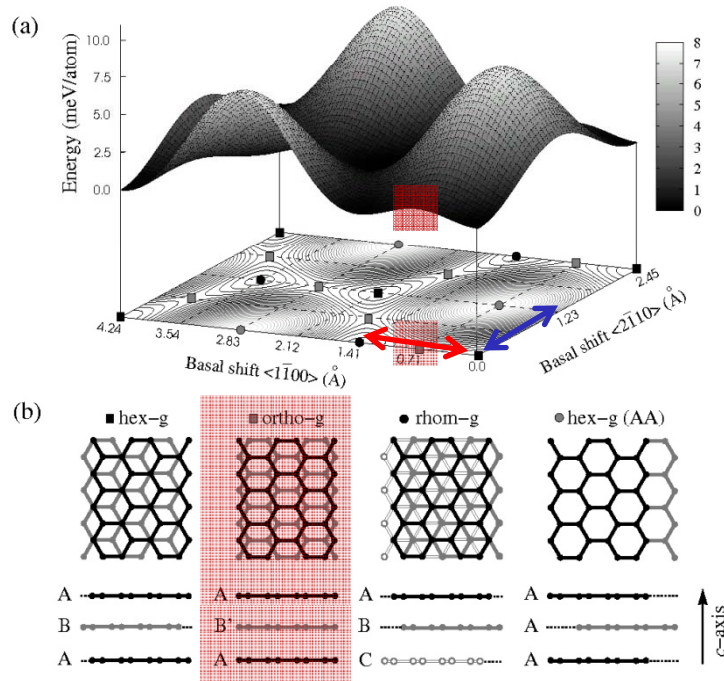


Figure 1: (a) Stacking-fault energy surface. The square and circle symbols indicate the stationary points corresponding to the following high-symmetric structures; (b) The hexagonal, orthorhombic, rhombohedral and AA hexagonal graphite viewed perpendicular (above), parallel (below) to the c -axis.

	a_0 [Å]	\bar{c}_0 [Å]	E_f [meV/atom]
hex-g (AB)	2.450	3.34	0.00 (0.00)
rhombo-g	2.450	3.34	0.10 (0.10)
turbo-g	2.450	3.42	3.03 (4.63)
ortho-g	2.450	3.37	1.66 (2.05)
hex-g (AA)	2.450	3.60	9.29 (7.70)

Table I: Intralayer a_0 and interlayer \bar{c}_0 repeat distances for the five graphitic systems. The last column shows the relative formation energies E_f per atom. The value between brackets are calculated using the van der Waals corrections.

Our work:

$$C_{44} = -2.7 \text{ GPa} \quad \text{— red line —}$$

$$C_{44} = 7.7 \text{ GPa} \quad \text{— blue line —}$$

$$C_{13} = -2.6 \text{ GPa}$$

Results

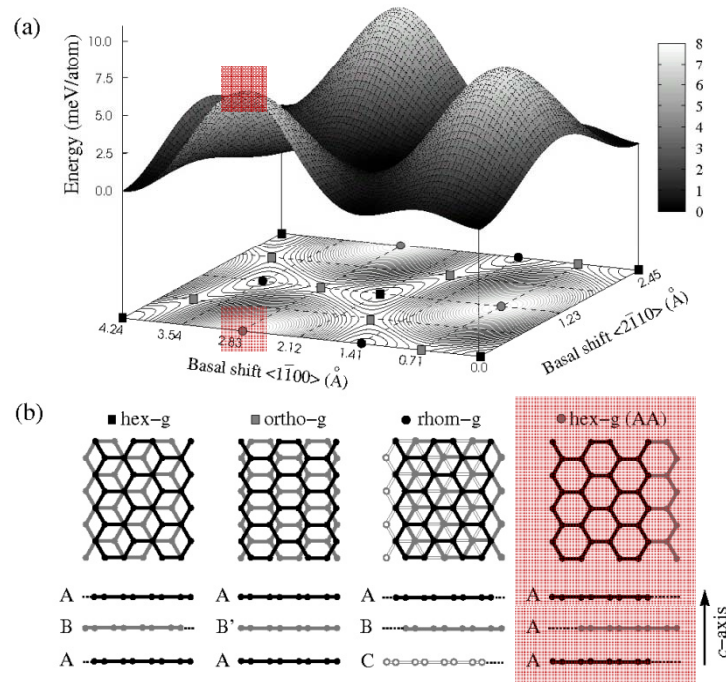


Figure 1: (a) Stacking-fault energy surface. The square and circle symbols indicate the stationary points corresponding to the following high-symmetric structures; (b) The hexagonal, orthorhombic, rhombohedral and AA hexagonal graphite viewed perpendicular (above), parallel (below) to the c -axis.

	a_0 [Å]	\bar{c}_0 [Å]	E_f [meV/atom]
hex-g (AB)	2.450	3.34	0.00 (0.00)
rhomb-g	2.450	3.34	0.10 (0.10)
turbo-g	2.450	3.42	3.03 (4.63)
ortho-g	2.450	3.37	1.66 (2.05)
hex-g (AA)	2.450	3.60	9.29 (7.70)

Table I: Intralayer a_0 and interlayer \bar{c}_0 repeat distances for the five graphitic systems. The last column shows the relative formation energies E_f per atom. The value between brackets are calculated using the van der Waals corrections.

Our work:

$$C_{44} = -3.8 \text{ GPa}$$

$$C_{13} = -3.0 \text{ GPa}$$

Results

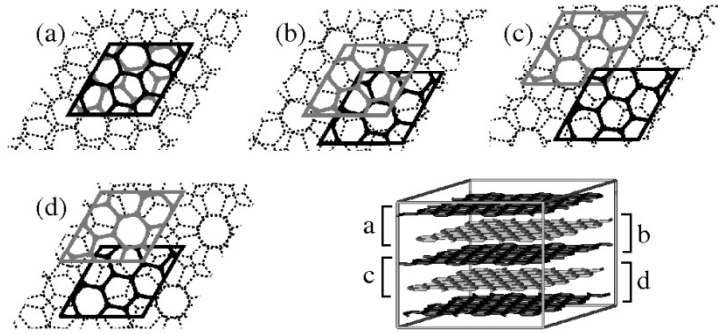


Figure 1: An example of turbostratic stacking. Each layers is rotated with respect to each other with a fixed angle of 38.21° and randomly translated along the basal plane.

Results

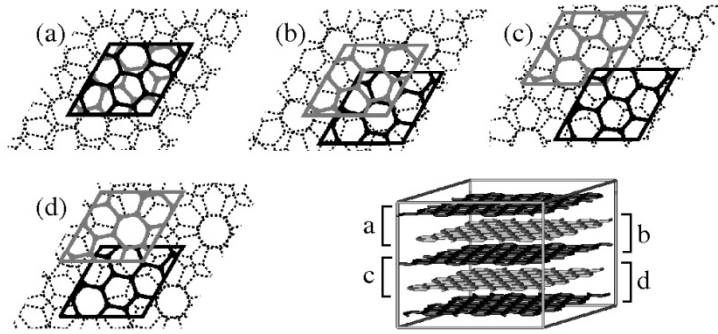


Figure 1: An example of turbostratic stacking. Each layers is rotated with respect to each other with a fixed angle of 38.21° and randomly translated along the basal plane.

	a_0 [\AA]	\bar{c}_0 [\AA]	E_f [meV/atom]
hex-g (AB)	2.450	3.34	0.00 (0.00)
rhomb-g	2.450	3.34	0.10 (0.10)
turbo-g	2.450	3.42	3.03 (4.63)
ortho-g	2.450	3.37	1.66 (2.05)
hex-g (AA)	2.450	3.60	9.29 (7.70)

Table I: Intralayer a_0 and interlayer \bar{c}_0 repeat distances for the five graphitic systems. The last column shows the relative formation energies E_f per atom. The value between brackets are calculated using the van der Waals corrections.

Results

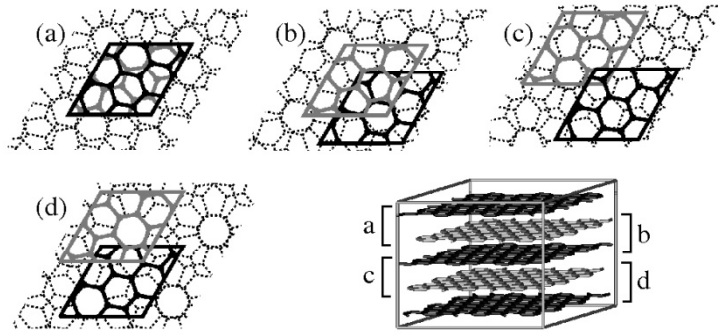


Figure 1: An example of turbostratic stacking. Each layers is rotated with respect to each other with a fixed angle of 38.21° and randomly translated along the basal plane.

	a_0 [Å]	\bar{c}_0 [Å]	E_f [meV/atom]
hex-g (AB)	2.450	3.34	0.00 (0.00)
rhomb-g	2.450	3.34	0.10 (0.10)
turbo-g	2.450	3.42	3.03 (4.63)
ortho-g	2.450	3.37	1.66 (2.05)
hex-g (AA)	2.450	3.60	9.29 (7.70)

Table I: Intralayer a_0 and interlayer \bar{c}_0 repeat distances for the five graphitic systems. The last column shows the relative formation energies E_f per atom. The value between brackets are calculated using the van der Waals corrections.

Our work:

$$C_{44} = 0.24 \pm 0.06 \text{ GPa} \quad (\text{Exp. } 0.18 - 0.35 \text{ GPa})$$

$$C_{13} = -2.7 \pm 1.0 \text{ GPa} \quad (\text{Exp. } 15 \pm 5 \text{ GPa})$$

↗ Ultrasound experiments

↘ Static test methods
Less accurate !!

Results

$$B_a = \frac{C_{33}(C_{11} + C_{12}) - 2C_{13}^2}{C_{33} - C_{13}}$$

$$C_{13} = 0 \text{ GPa}$$



$$B_a = 1240 \text{ GPa}$$

$$C_{13} = 15 \text{ GPa}$$



$$B_a = 2080 \text{ GPa}$$

Results

$$B_a = \frac{C_{33}(C_{11} + C_{12}) - 2C_{13}^2}{C_{33} - C_{13}}$$

$$C_{13} = 0 \text{ GPa} \quad \longleftrightarrow \quad B_a = 1240 \text{ GPa}$$

$$C_{13} = 15 \text{ GPa} \quad \longleftrightarrow \quad B_a = 2080 \text{ GPa}$$

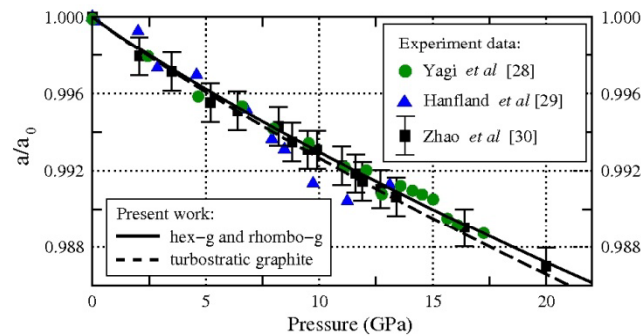


Figure 1: In-plane lattice parameters *vs.* pressure. The solid line represents the results found for hex-g and rhombo-g. The dashed line shows the result found for turbostratic graphite. For comparison, the experimental results are also plotted.

T. Yagi *et al.*, Phys. Rev. B **46**, 6031 (1992).

M. Hanfland *et al.*, Phys. Rev. B **39**, 12598 (1989).

Y.X. Zhao *et al.*, Phys. Rev. B **40**, 993 (1989).

- The powder samples are ranging from well crystallized to poorly crystallized grains
- The good agreement indicate that B_a does not depend on the stacking order.
- The measured value is:

$$B_a = 1250 \text{ GPa} \quad C_{13} = 0.3 \text{ GPa}$$

Results

$$B_a = \frac{C_{33}(C_{11} + C_{12}) - 2C_{13}^2}{C_{33} - C_{13}}$$

$$C_{13} = 0 \text{ GPa} \quad \longleftrightarrow \quad B_a = 1240 \text{ GPa}$$

$$C_{13} = 15 \text{ GPa} \quad \longleftrightarrow \quad B_a = 2080 \text{ GPa}$$

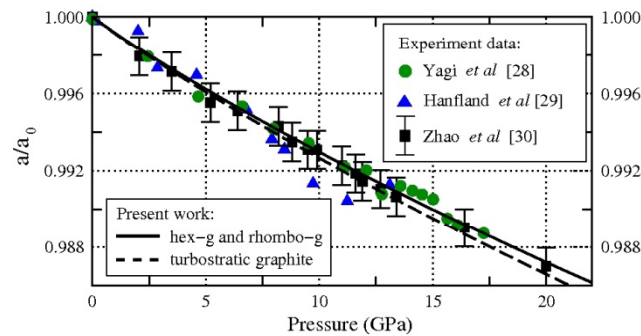


Figure 1: In-plane lattice parameters *vs.* pressure. The solid line represents the results found for hex-g and rhombo-g. The dashed line shows the result found for turbostratic graphite. For comparison, the experimental results are also plotted.

T. Yagi *et al.*, Phys. Rev. B **46**, 6031 (1992).

M. Hanfland *et al.*, Phys. Rev. B **39**, 12598 (1989).

Y.X. Zhao *et al.*, Phys. Rev. B **40**, 993 (1989).

- The powder samples are ranging from well crystallized to poorly crystallized grains
- The good agreement indicate that B_a does not depend on the stacking order.
- The measured value is:

$$B_a = 1250 \text{ GPa} \quad C_{13} = 0.3 \text{ GPa}$$

We propose that the same value found in hex-g $C_{13} = 0 \pm 3 \text{ GPa}$ should be appropriate also for turbo-g.

Results

	hex-g (AB)		turbo-g		rhombo-g	ortho-g	hex-g (AA)
	Experiment	Theory	Experiment	Theory	Theory	Theory	Theory
C_{11}	1109 ± 16	1109	1060 ± 20	1080 ± 3	1107	1095	1028
C_{12}	139 ± 36	175	180 ± 20	171 ± 4	175	173	162
C_{33}	38.7 ± 7	29 (42)	36.5 ± 1	27 ± 2 (36 ± 1)	29 (42)	26 (38)	21 (30)
C_{13}	0 ± 3	-2.5	15 ± 5	-2.7 ± 1	-2.5	-2.6	-3.0
C_{44}	5.0 ± 3.0	4.5 (4.8)	0.18 / 0.35	0.24 \pm 0.06 (0.27 \pm 0.05)	4.4 (4.8)	-2.7/7.7 (-2.9/7.3)	-3.8 (-3.8)

Table I: Elastic constants in unit of GPa for different graphitic systems. The values between brackets are calculated using the van der Waals correction. We have shown that the C_{13} values do not significantly change between turbo-g and hex-g and we have proposed that the same value 0 ± 3 GPa should be appropriate also for turbostratic stacking.

- The lower exfoliation energy and the lower C_{44} (more bending modes) suggest that flakes with random stacking should be easier to exfoliate than the ones with perfect or rhombohedral stacking in agreement with a recent experiment [1];
- The bending modes may contribute to decouple the layers giving rise to a quasi 2D electronic systems in turbostratic graphitic systems;

[1] Y. Hernandez *et al.*, Nature Nanotech. 3, 563 (2008).

Conclusions

1. We have explained the importance of C_{44} as the main parameter that controls the bending branch and mechanical stability in graphitic systems;
2. We have provided the first complete description of the elastic constants in layered graphitic systems;
3. The higher formation energy (3-5 meV/atom) and the lower C_{44} value found in turbostratic graphite suggest that we could take advantage of this stacking to produce graphene samples in large scale.

Acknowledgements

HPC-Europa project

My collaborators:

Annalisa Fasolino and Mikhail I. Katsnelson, Nijmegen, The Netherlands

Y. Dappe, Madrid, Spain (van der Waals implementation)

J-C Charlier, Belgium

S. Öberg, Luleå, Sweden

Acknowledgements

Thank you

